Establishing confidence in predictions of fatigue loading for floating tidal turbines based on large-eddy simulations and unsteady blade element momentum

P. Ouro, H. Mullings & T. Stallard
School of Engineering, The University of Manchester, UK

ABSTRACT: To optimise a tidal site for development, tidal stream turbines need to be placed within arrays with the spacing between turbines being critical to maximise energy yield whilst minimising expenses associated to cabling, mooring or maintenance. Turbines deployed downstream of other turbines are exposed to upstream turbine wakes. experiencing low velocities and high shear and turbulence which cause fatigue loads. Turbine loading due to these challenging conditions can be well-predicted using high-fidelity models such as Large-Eddy Simulation (LES). However, such models have a notable computational cost that prevents use for optimising the location of turbines within an array. Here, we investigate the accuracy of a computationally efficient Blade Element Momentum (BEM) to predict unsteady loads on a double-rotor floating tidal turbine, adopting inflow data from LES and comparing to loads resolved in the LES using an Actuator Line Model (ALM). Results show that mean thrust and bending moment are well predicted by the BEM in comparison to the LES-ALM results.

1 INTRODUCTION

A number of tidal stream turbine designs, typically adopting a horizontal axis rotor, have now been trialled at full-scale and the development of tidal arrays is ongoing for sites in the UK, France and Canada. As this renewable energy sector continues to develop, further research is required in the design of turbines for operation within arrays. Different environmental factors influence unsteady loading of individual turbines and their components depending on whether these are bottom-fixed or floating devices (Stansby and Ouro 2022, Mullings and Stallard 2021). Floating tidal turbines benefit from operating in the higher velocity flows that typically occur near surface, and from easier access for maintenance but are subjected to wave loading (Díaz-Dorado et al. 2021). Conversely, bottom-fixed turbines are static without a mooring system and avoid the action of waves for most conditions, but are subjected to bathymetry-induced turbulence (Parkinson & Collier 2016, Ahmed et al. 2017, Harrold & Ouro 2019, Ouro & Stoesser 2019, Mercier et al. 2020).

Accurate prediction of onset flows - which can be a complicated mixture of shear, turbulence and waves - and of resultant turbine loading is required for the design of tidal turbine arrays as these onset conditions define energy yield per turbine and component fatigue life. The variation of onset flow characteristics, caused by such environmental factors, can include a range of flow speeds and vertical profiles as well as different turbulence parameters, such as intensity and length-scale (Togneri & Masters 2016, Garcia-Novo & Kyozuka 2019) and, for near-surface turbines in particular, surface waves. Each individual turbine will be affected by the onset flow, however if there is a large array then each turbine will also be subject to the effects of blockage generated between turbines and wakes from upstream devices (Ouro & Nishino 2021). By understanding and predicting the different loading patterns, more accurate design life can be estimated along with overall performance.

For engineering design the estimation of loadings on a tidal rotor is normally assessed via Blade Element Momentum (BEM). A key feature of this method is the low computational cost. Accuracy has also been demonstrated for experimental studies and relative to the operating loads on trial full-scale turbines (Parkinson & Collier 2016, Harrold et al. 2020) with well-defined inflow conditions. Explicit computational simulations of tidal turbines have also been used for analysis of turbine loading, onset flows and resultant wakes. Such models resolve the fluid flow in three-dimensional domains with a given turbulence closure, e.g. Reynolds Averaged Navier-Stokes (RANS) or Large-Eddy Simulation (LES). The former provides time-averaged results and models the turbulence (Apsley & Stansby 2020) whilst the latter enables the resolution of the turbulence structures larger than the grid size (Posa & Broglia 2021). Within these models, a turbine rotor can be fully resolved, or more typically due to the lower computational cost, represented with an Actuator Line Method (ALM) to capture tip vortices and the far-wake. The LES-ALM is becoming a suitable numerical approach to compute the loadings on the rotor and resolve the turbine wake (Ouro & Nishino 2021).

This work focuses on studying the loading on a 20 m diameter two-rotor floating tidal turbine, (Orbital Marine Power 2022), under conditions similar to those found at a tidal site using an LES-ALM for loading and wake analysis and from which instantaneous velocity data is extracted to provide inflow to a BEM. The use of the downstream onset flow planes allows for the determination of the loading for a second device when placed at different downstream locations using the unsteady BEM which, if accurate, can remove the need for running multiple LES cases. The ability of BEM to predict thrust and bending moments at almost no computational cost will be compared to those predicted by the LES-ALM, to inform complementary use of both types of model for the design of turbine arrays.

2 NUMERICAL MODELS SET-UP

2.1 *Turbine Models*

2.1.1 *Blade Element Momentum Theory*

The tidal device modelled here consists of two rotor each with two blades, following the design of a full-scale floating device by Orbital Marine Power (Orbital Marine Power 2022). Modelling turbines computationally can be performed in different ways and have been introduced in Section 1, in this work two of these models are used and their results compared. Firstly, blade element momentum theory has been applied to both the steady and unsteady conditions. The BEM employed here extracts the onset flow at 'N' positions along a blade length, which rotate with time, depending on the chosen operating point. The onset flow is used to determine the relative onset flow (U_{rel}) and inflow angle (ϕ) to the blade at each position along the blade, as shown by Equations 1-2.

$$\delta U_{rel}(t) = \sqrt{U_X^2 + (\Omega r - U_\Theta)^2)} \tag{1}$$

$$\delta\phi(t) = sin^{-1}\frac{U_X(t)}{U_{rel}(t)} \tag{2}$$

Where U_{rel} is the relative velocity to the blade which incorporates the longitudinal velocity, U_X is the stream-wise onset velocity which includes in axial induction (a) through $U_X = U_0(1-a)$ and the components in the tangential direction, U_Θ with the angular velocity ω and each radius r. The lift and drag force on each blade segment vary according to Equations 3-4.

$$\delta L(t) = \frac{1}{2}B\rho c(U_{rel})^2 C_L \delta r \tag{3}$$

$$\delta D(t) = \frac{1}{2}B\rho c(U_{rel})^2 C_D \delta r \tag{4}$$

Where c is the chord length, δr is the radial width of the blade segment, B is the number of blades, ρ is the fluid density, C_L and C_D correspond to the lift and drag coefficients respectively. Using the calculated lift and drag forces for each blade the axial (F_a) and tangential (F_t) forces along each blade are calculated using Equations 5-6.

$$\delta F_a(t) = \delta L(t)cos(\phi(t)) + \delta D(t)sin(\phi(t)) \tag{5}$$

$$\delta F_t(t) = \delta L(t)sin(\phi(t)) - \delta D(t)cos(\phi(t)) \tag{6}$$

The axial force (F_a) on each segment of the blade leads to the calculation of root bending moment as well as rotor thrust. These results can be used to establish the respective load spectra and hence determine the load cycles enabling the fatigue loads to be predicted for the blades and rotor.

An initial comparison is conducted using a steady case, a tip-speed-ratio (TSR) of 5.5 is chosen, resulting in peak C_P values, representative of a full-scale device (McNaughton, Harper, Sinclair, & Sellar 2015) and with a difference of only 7%, and a 0.5% difference in C_T between the two methods.

2.1.2 *DOFAS*

The Digital Offshore FArms Simulator (DOFAS) in-house code adopts the large-eddy simulation (LES) turbulence closure to resolve the turbulent scales larger than the grid size, capturing the energetic large-scale vortices from tidal flows and those turbulent structures introduced by tidal turbines (Ouro et al. 2019). DOFAS adopts an actuator line method with an anisotropic interpolation procedure that provides an improved force communication between fluid and structural meshes (Ouro & Nishino 2021), and also adopts a Prandtl correction to account for tip losses (Shen et al. 2005). The use of ALM enables the use of relatively coarse grid resolutions without the need for explicitly resolving the rotor geometry, which alleviates the computational cost of LES (Stansby & Ouro 2022). The accuracy of this LES-ALM approach in DOFAS was validated in terms of hydrodynamic coefficients and wake characteristics in Ouro et al. (2019) for small-scale tidal turbine arrays.

A uniform grid resolution (Δx) of 0.375 m in the three spatial directions is adopted, yield a number of grid cells per direction of 1920×672×112, i.e. 144 million cells. A fixed time step is kept to 0.0475 s and 70,000 time steps are computed to simulate more than 3,300 s of physical time using 200 CPUs on the

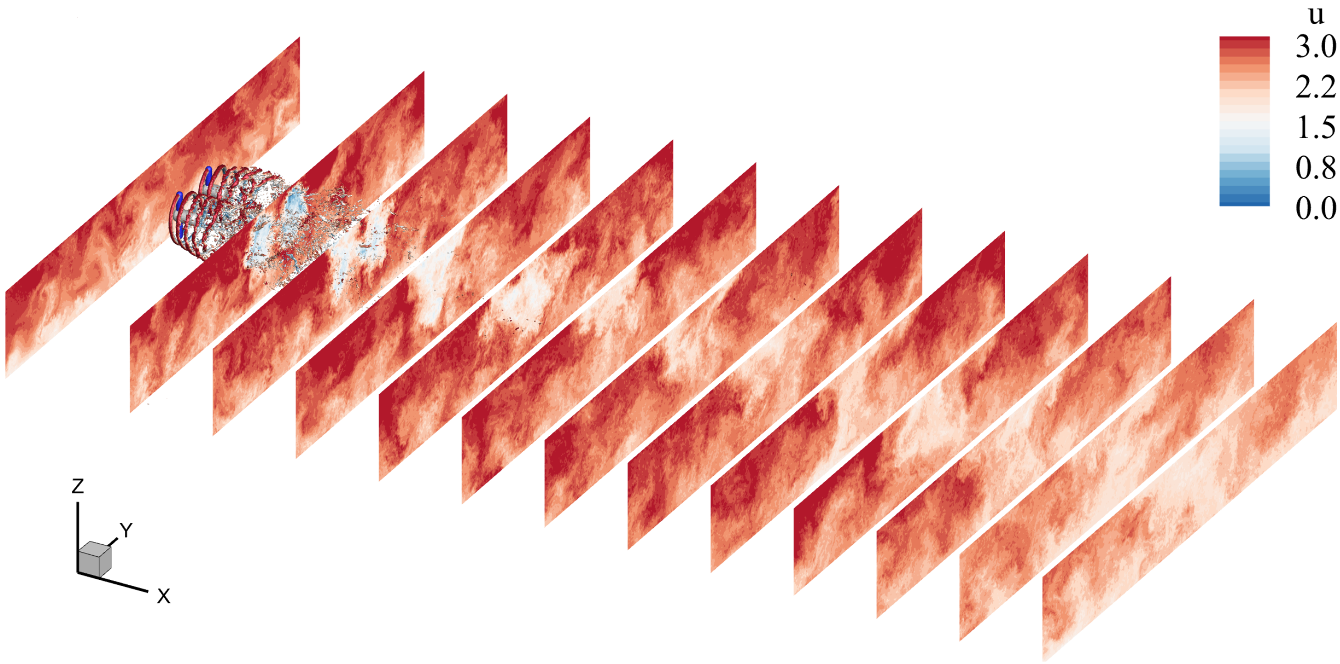

Figure 1: Positions of yz-planes with contours of instantaneous streamwise velocities generated from the LES of the two-rotor tidal turbine with turbulent structures represented using the Q-criterion.

local CSF cluster at The University of Manchester. At the inlet, a $1/7^{th}$ power-law vertical shear profile with a mean velocity of 2.5 m/s at hub height is adopted with an imposed turbulence intensity of 10% as typically found at tidal sites, which was generated using an anisotropic Synthetic Eddy Method (SEM) with length-scales of 50 m, 20 m and 15 m, in x-, y- and z-direction respectively.

2.2 *Onset Flow Conditions*

2.2.1 *Single Device*

This study models a floating tidal turbine device comprising two rotors with a $0.25D$ (diameter) transverse spacing (y_s) operating at peak performance (not disclosed due to confidentiality). Each rotor has a diameter of 20 m, with a hub height location 13 m below the mean water level of a typical tidal site, here the depth is modelled at 42 m. This provides a depth-to-diameter ratio of approx. 2. The computational domain modelled using DOFAS measures 720 m, 252 m and 42 m in streamwise, transverse and vertical directions, with turbines placed at 230 m from the inlet and centred in the lateral direction, representing full-site test conditions. The grid resolution provides 53 mesh cells per rotor diameter ($\Delta x/D$) which is adequate to represent the rotor-induced turbulence (Ouro et al. 2019).

The LES is hot-started for 6,000 time steps to cover approx. 300 s during which yz-planes containing instantaneous velocity components are extracted at various streamwise positions from -1D until 22D downstream, as shown in Figure 1 with streamwise velocities (u). This LES inflow data is used here as unsteady onset flow to both turbine models, with the ALM included as part of the LES simulation. The onset flow for the BEM is therefore extracted one diameter upstream of the modelled device. These planes are used as input to the BEM to determine the difference in loading from each method. Using the ALM within the LES results in a wake caused by the device, this wake can accurately describe the downstream conditions as shown in Ouro et al. (2019).

The cross-section normal to the flow direction of the LES domain at 1D upstream of the tidal turbine is shown in Figure 1 with contours of stream-wise velocities. This depicts that this setup is wide enough to enable the inclusion of two additional turbine rotors to allow for the investigation of secondary floating turbines placed within the wake of the upstream devices.

Across the domain, the LES-computed vertical time-averaged velocity profiles are determined at the two rotor positions and shown in Figure 2, which are well represented by the theoretical vertical shear profile. It is worth noting that across the floating rotor position (-3 m$< z <$-23 m) there is less variation in velocities due a reduced vertical shear than compared to a lower bed mounted device.

In addition to the changes in mean velocity recreated within the onset flow simulation, the spatial variation of turbulence characteristics are also observed across the domain as shown in Figure 3 with contours of turbulence intensity ($TI = u'/U_0$, with u' denoting time-averaged velocity fluctuations and U_0 is the bulk velocity equal to 2.5 m/s) at one diameter upstream of the turbine rotors.

As seen in Figure 3 the TI across the domain is not constant at the pre-defined value, due to the influence of the bed contributing to introduce turbulence within the lower part of the domain in addition that from the unsteady SEM inflow used in the LES. Across the ro-

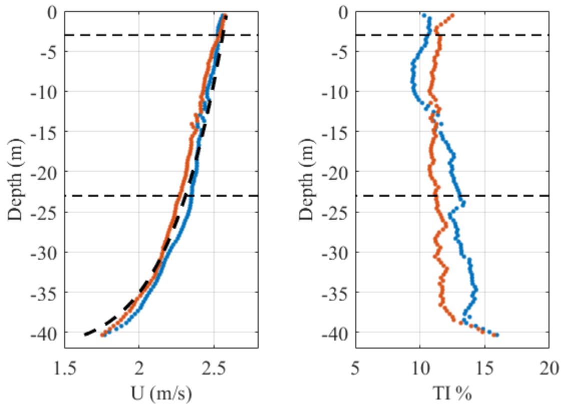

(a) (b)

Figure 2: Upstream depth profiles of average stream-wise velocity at the centre of each rotor position (orange/blue), compared to the defined $1/7^{th}$ shear profile (black dash).

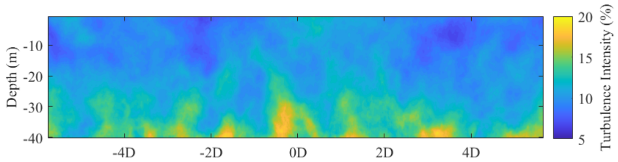

Figure 3: Cross section at 1 diameter upstream of the tidal device, showing the spatial variation of streamwise turbulence intensity within the LES.

tor planes, vertical profiles of TI are shown in Figure 2, where rotor one experiences a range from 9.5-13% and rotor two is more constant around 11%, with rotor one on the left when facing the device from an upstream position. Such differences between locations are because the onset planes cover a period of 300 s that might not provide fully converged turbulence statistics but are representative of the mean flow.

2.2.2 *Devices in the downstream wake*

The floating tidal turbine wake characteristics are evaluated to determine the flow conditions as though another two-rotor device is placed at any location downstream. The disc-averaged value (U_{DA} is obtained by averaging the instantaneous velocities over the swept area of each rotor. Figure 4 depicts the location of a second set of rotors aligned with the original rotors in the lateral direction.

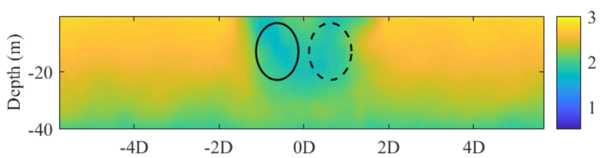

Figure 4: Variation of disk averaged velocity (U_{DA}) with both downstream and transverse device position, rotor one (solid line) and rotor two (dashed line).

The disc-averaged velocity is evaluated at five spanwise positions (y) with the centre of the two-rotor turbine at $0D$, $1D$, $2D$, $3D$, and $4D$, and at 10 downstream positions ranging from $6D$ until $24D$ every $2D$. The results of U_{DA} are shown in Figure 5 for both turbine rotors. In a fully aligned configuration, i.e. $y = 0D$, both rotors operate in a low-velocity region throughout the wake extension. Adopting a separation of $y = 1D$ enables the second rotor to operate in a more energetic region (see Figure 4) with high U_{DA} values in the near wake which decrease further downstream due to the transverse wake expansion (Stallard, Feng, & Stansby 2015), converging to the free-stream value. Figure 5 indicates that when the second turbine is located in the bypass region there is a velocity increase up to $12D$ downstream that could lead to an increase in performance (Ouro & Nishino 2021).

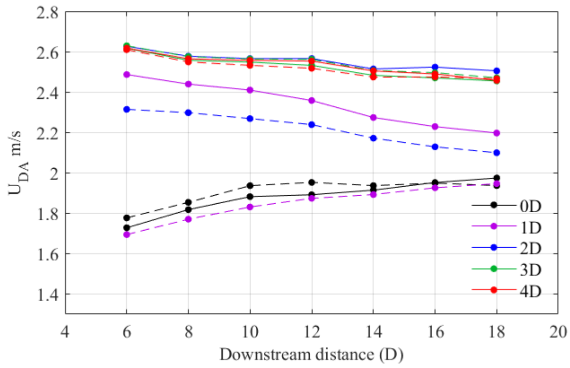

Figure 5: Variation of disk averaged velocity (U_{DA}) with both downstream and transverse device position, rotor one (solid line) and rotor two (dashed line).

Overall, the U_{DA} values in Figure 5 indicate that the wake is almost recovered after $18D$ downstream of the two-rotor system. If the characteristic length of the two-rotor device is deemed as $D_2 = 2{\cdot}D + y_s = 45$ m, this downstream distance is approx. $8D_2$, which seems a more reasonable reference for scaling the wake dynamics.

An analogous analysis is done for the disc-averaged turbulence intensity (TI_{DA}) presented in Figure 6 for the different downstream positions evaluated. These results evidence that devices operating in fully-waked conditions experience a highly unsteady flow dynamics with TI values exceeding 20% even $12D$ downstream.

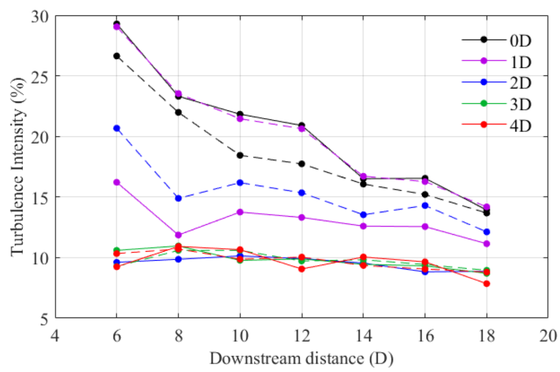

Figure 6: Variation of disk averaged stream-wise turbulence intensity (TI_{DA}) with both downstream and transverse device position, rotor one (solid line) and rotor two (dashed line).

Although tidal sites experience a variety of different shear and turbulence characteristics (Milne et al. 2016, Lewis et al. 2017, Garcia-Novo & Kyozuka 2019), the purpose here is to establish confidence in the loading predictions from this specific set of conditions which best represent this device at optimum power production.

3 LOADING ON A SINGLE DEVICE

The blade and rotor loads from each modelling method for the two rotors on the single device are discussed in this section. The time varying thrust loading on each rotor is calculated from the combined axial force on the two blades, and shown in Figure 7.

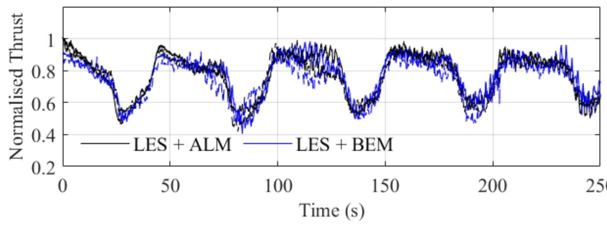

Figure 7: Varying thrust loading with time for the ALM (black) and BEM (blue), rotor one (solid lines) and rotor two (dashed lines).

The time varying thrust has been normalised by the maximum value across all four cases (two methods, two rotors). Overall, the thrust loading determined by each method shows very good agreement, both in phase at the same magnitudes. This is confirmed by the mean thrust loading and hence mean C_T being within 2%. A slight increase in the difference than for the steady case, but when considering the variation of inflow condition the BEM is capturing the unsteady load fluctuations well.

The root bending moment is calculated using the axial loading on the blade and within the BEM using the Simpson's rule to integrate forces along the blade to obtain the flapwise bending moment. A comparison of the calculated bending moments between the two methods is shown in Figure 11. The mean loading across these cases varies by 10% between the two turbine modelling methods, with the ALM including tip loss correction which is not implemented in the BEM method.

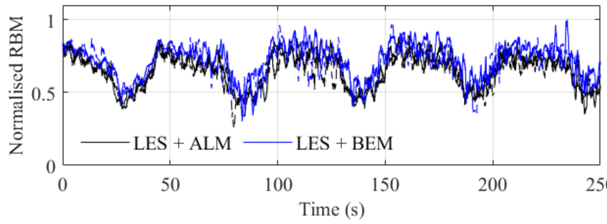

Figure 8: Varying root bending moment with time for the ALM (black) and BEM (blue), rotor one (solid lines) and rotor two (dashed lines).

When examining the time varying loading the fluctuations caused by the onset turbulence can be seen, but the magnitude is more difficult to distinguish. Therefore the load spectra for both sets of loading results is shown in Figures 9–10, in which the rotor frequency (f_0) is used to normalise the frequencies. Both methods are shown to capture that the main thrust variation in the rotor occurs at the blade passing frequency (equal to $2f_0$) with a pronounced harmonic at twice that frequency. The energy associated to those events is similar between the LES-ALM and LES-BEM.

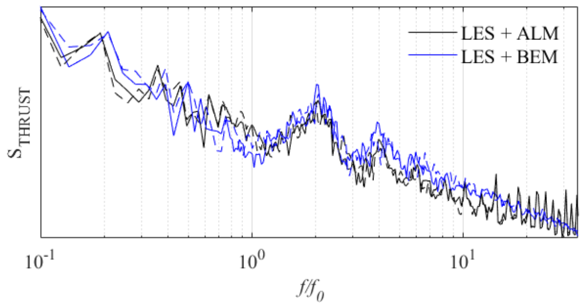

Figure 9: Thrust loading spectra determined from both turbine modelling methods, ALM (black and BEM (blue), rotor one (solid lines) and rotor two (dashed lines).

In the case of the bending moment spectra, the most energetic peak is observed at the blade passing frequency with secondary peak at its harmonic. The energy decay at the higher frequencies is very similar between both methods, with slightly higher values for the BEM case. For both loading spectra shown, the LES onset flows are considered using Taylor's Hypothesis of frozen turbulence for the BEM case, this results in the reduction in spikes in the spectra at the high frequency range. Overall though the BEM methods has produced a load spectra which well represents the load variation using the ALM method within the computational LES domain.

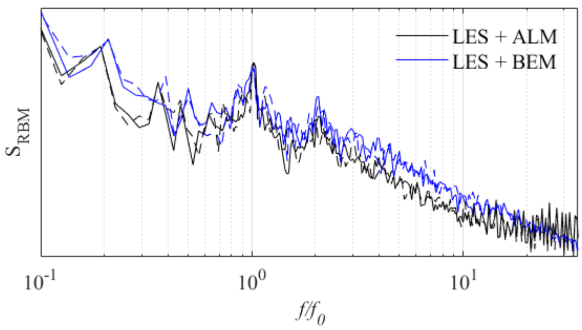

Figure 10: Root bending moment spectra determined from both turbine modelling methods, ALM (black and BEM (blue), rotor one (solid lines) and rotor two (dashed lines).

In addition to looking at the time history of loads and the loading spectra the azimuthal variation shows a clear representation of what conditions the turbine blades are experiencing as they rotate. The azimuthal variation for the one blade on each rotor is shown in Figure 11. For this upstream device the normalised RBM is showing the influence of the applied $1/7^{th}$

power law vertical shear profile, with minimal loading when the blade is positioned vertically downwards at 180^D. Between the two rotors, rotor one is showing a slight increase in the loads experienced through the rotation, but this difference is around 2%.

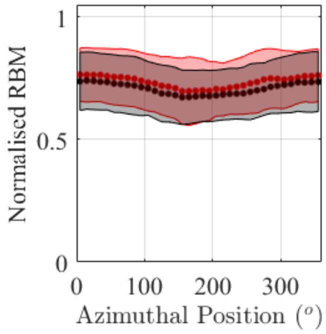

Figure 11: Azimuthal variation of the root bending moment for one blade on each rotor within the device, rotor one (red) and rotor two (black), where the mean variation is shown by dots and the variation within one standard deviation given by the shaded area.

4 VARIATIONS OF LOADS IN WAKES

This section examines the variation in loading when considering a additional turbine located downstream of the original device. Utilising the velocity deficit in the wake caused by the ALM within the LES. In this case the additional device is kept at the same operating point, TSR of 5.5, the angular speed of the additional turbines is determined based on the mean onset flow velocity, which has been shown in Figure 5. As shown in this figure the disk averaged velocity at the different downstream positions varies due to the wake deficit and transverse position of the turbine.

4.1 *In-line Devices*

Initially the loading experienced on the device directly inline of the original upstream device is determined. Figure 12 shows the load spectra of thrust for three downstream wake positions as well as the initial upstream case from Figure 9, for clarity in these comparisons, thrust loading on one rotor from the device is shown.

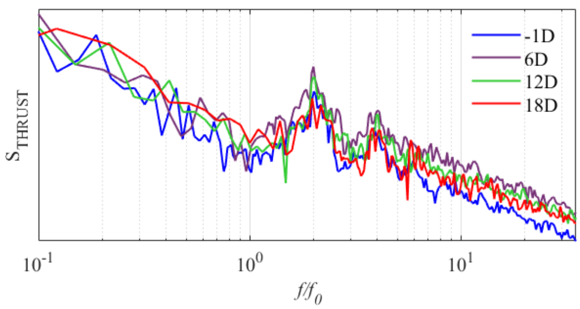

Figure 12: Load spectra for the thrust variation with downstream position for another device inline with the upstream at various downstream positions.

The loading for all the devices in-wake are determined using the BEM method only. Considering a device operating in the wake of the upstream, the three positions are chosen to represent the closest a turbine would realistically be located, the furthest downstream and midway between. Based on the disk averaged conditions shown in Section 2.2.2 the velocity and turbulence intensity varies considerably across these positions, with a reduction in intensity values and an increase in velocity. The greatest variation between the upstream conditions and the in-wake positions is found for the 6 diameter (6D) downstream case, this is as expected, based on the device experiencing the largest velocity deficit and device interaction with flow field to distort and alter the onset turbulence. This is also observed in the resultant loading spectra, for the thrust loading the peak magnitudes at the rotor frequency and subsequent first harmonic are clearly shown in Figure 12, with a difference in magnitude found across the upstream and three downstream cases. The largest peak magnitude found for the 6D downstream case and an increase in magnitude across the mid-high frequency range, corresponding to the increase in turbulence intensity. Further downstream at the 12D position the peak magnitude and overall spectral magnitude over the mid-high frequency range is has reduced from the 6D case but remains slightly greater than the 18D case. Again this change in magnitude corresponds to variation in the intensity observed at the downstream device positions. As shown in Section 2.2.2 at a downstream position of 18D for the two-rotor device corresponds to approximately 8D when considering a single rotor device, where the wake could still influence the downstream loading and performance. In this case the peak magnitudes for the 18D case are very similar to those determined for the upstream rotor, however the increase in spectral magnitude in the mid-high frequency range is still shown, as the turbulence intensity for this case is around 14%, not 10% which the upstream device experienced. The root bending moment spectra for the same device positions is shown in Figure 13, for one blade on one rotor.

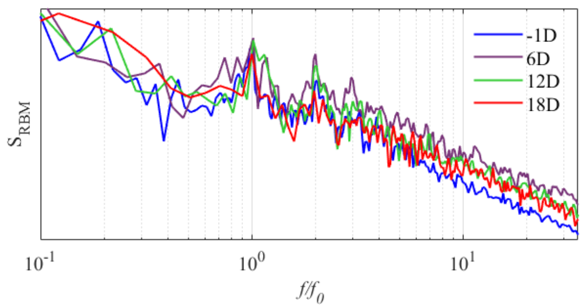

Figure 13: Load spectra of root bending moment for one blade on rotor one for the upstream device (blue) and three inline downstream device positions.

Following the root bending moment spectra for the single device, the downstream rotor shows the peak magnitudes at the rotor frequency and the first harmonic. As with the thrust spectra the 6D downstream device is showing the largest peak magnitude, showing that this device is experiencing the greatest variation in conditions, it also shows a peak at the second harmonic of the rotor frequency ($3f_0$), which is not observed with the upstream rotor or the further downstream cases (12/18D). The shift in magnitude over the mid-high frequency which was observed for the thrust spectra is also present with the spectra of root bending moment, caused by the increase in variance in the loading due to the turbulence intensity. It is worth noting here that the time history of loading for the 18 diameter case is shorter than the upstream turbine due to the length of time needed for the wake to reach the downstream position, the onset flow is only considered when the wake is fully established at each downstream position.

4.2 *Offset Devices*

In order to look at the loading in the wake of an upstream device, offset device locations also need to be explored. These offset positions are determined at each downstream location by positioning the device at different transverse locations, the locations are referred to by the notation 0D, 1D, 2D, 3D and 4D. In each case the D corresponds to the diameter as in the previous section and the each numerical values corresponds to shift left in the domain when facing the upstream turbine, which is considered to be placed at 0D. The average upstream velocity variation across the domain is shown in Figure 4, this domain is then captured in Figure 15, where it has been divided into the average onset flow experienced across the device at each transverse location, in addition the average turbulence intensity across the device positions is included.

The results from the in-line wake at 6D are shown in the previous section, here they are compared to each offset wake position and for each rotor position within the device. The load spectra of rotor thrust is shown in Figure 14, for both rotors, where the ‘0D’ case in (a) corresponds to the ‘6D’ case in Figure 12.

For both rotors the offset positions have resulted in a difference in load spectra. Rotor one is shown to have a similar peak magnitude and overall spectral magnitude over the mid-high frequency range, whereas the remaining three positions, (2D-4D), show reductions across the blade passing frequencies and the mid-high frequency range. These results are consistent with the average velocity and turbulence intensity shown in Figure 15. With the peak magnitudes impacted by the lack of shear as the rotor moves laterally out of the upstream wake and the spectral magnitude in the mid-high frequency range impacted by the reduction in turbulence intensity once this rotor reaches a 2D offset position. Based on this analysis it would be expected that the second rotor would experience higher peak and spectral magnitude across to the 2D offset position. When examining Figure 14(b) which shows the thrust loading for the second rotor, this is found, with the 2D offset position providing the greatest peak magnitude at the blade passing frequency and it’s harmonics, as well as a very similar magnitude to the 0D and 1D cases over the mid-high frequency range. When comparing the load spectra between the two rotors at each transverse position, 2D has the largest variation in peak magnitude, caused by the shear and TI variation experienced on rotor two compared to rotor one. The far offset cases (3D-4D) experience the same onset flow conditions which has resulted in repeatable load spectra, which should correspond with load spectra from the upstream device. However although the peak magnitudes correspond between the three cases, showing the device experiences a similar onset shear, the magnitude at the mid-high frequency range is greater for the 3D and 4D offset cases. A similar turbulence intensity is shown in Figure 6, perhaps a slight increase for the offset over the original 10% considered for the upstream case, but a greater disk averaged onset flow is experienced on the offset cases due to the blockage within the domain, increasing the flow in the bypass which is onset to the 3D and 4D cases.

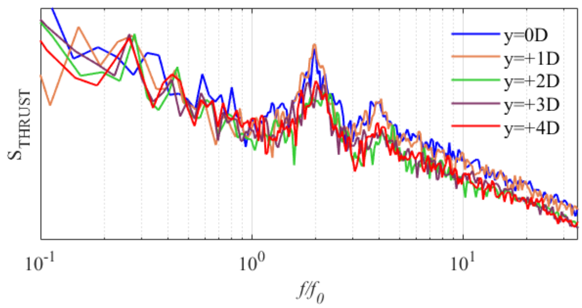

(a) Rotor One

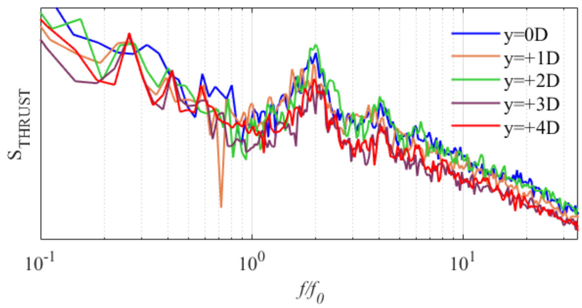

(b) Rotor Two

Figure 14: Thrust load spectra for various offset wake positions, for (a) rotor one and (b) rotor two.

In addition to determining the load spectra the mean loads is also compared between the two rotors at each offset position. For the 3D and 4D cases there is less than a 2% difference in the thrust coefficient between these cases, which is consistent with the observations from the load spectra. For in-line case

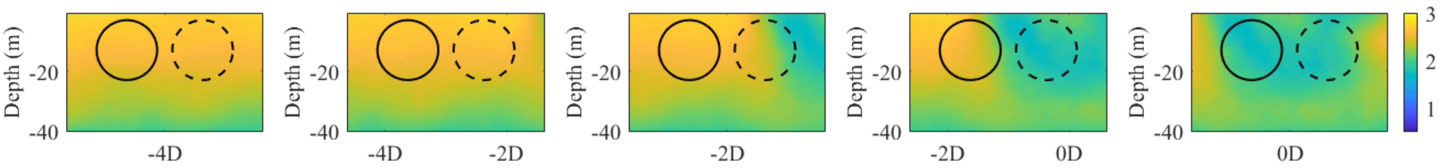

(a) Average Stream-wise Velocity

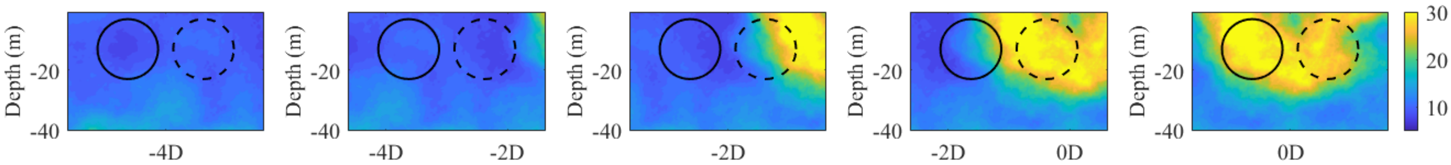

(b) Stream-wise Turbulence Intensity

Figure 15: Two rotor device across the domain, left to right: 4D to 0D at a position 6 diameters downstream of a device, with each rotor position outlined in black, rotor one (solid line) and rotor two (dashed line) for (a) Time-averaged velocity and (b) Turbulence intensity.

this increases slightly to a 7% difference, expected with greater variations in the peak magnitude and the greater difference in turbulence shown by Figures 6 and 15. The mean loading on the 2D offset case also varies by 8%, but the difference for the 1D case is greater at 17%. When examining the load spectra in Figurerotorth both rotor are shown in experience TI at a similar value to the inline case, however Figure 6 shows that rotor one experiences an average TI of 16% compared to rotor two which is around 29%. This difference in TI is also shown in Figure 15, where the offset of the device is resulting in rotor two moving across into the wake of the upstream rotor one. For these five transverse locations the root bending moment on the blades has been determined, the load spectra for each rotor is shown in Figure 16.

By analysing the load spectra for the root bending moment the rotational variation due to shear can be determined. As with the load spectra for thrust the '0D' case is a repetition from the previous inline wake for '6D', shown in Figure 13. One blade on each rotor has been shown for clarity. Considering rotor one, it is clear that the by offsetting this turbine by 1D has resulted in an increase to the shear that is experienced on the rotor, providing a greater peak magnitude at the rotor frequency and it's harmonics. The overall magnitude in the spectra over the mid-high frequency range is also consistent with the 0D case and the turbulence intensity results shown in Figure 6. Following on from the load spectra results for the thrust, the remaining offset wake cases have a reduced spectral magnitude related to the decrease in turbulence intensity, however the peak magnitude is similar to the inline case, demonstrating that the blade is still rotating through a sheared velocity profile. In comparison with rotor one, the most dominant peak loading is experienced by the 2D offset case for rotor two, shown in Figure 16(b). This is due to the blade operating

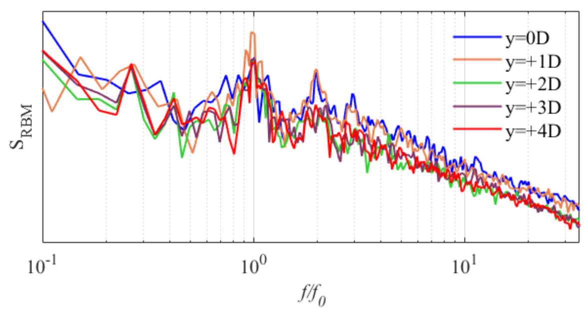

(a) Rotor One

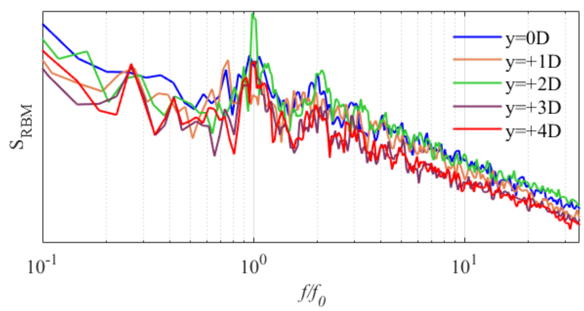

(b) Rotor Two

Figure 16: Root bending moment load spectra for various offset wake positions, for one blade on each rotor.

through a greater shear profile than any other rotor position, and is shown by the middle velocity contour in Figure 15(a). At the 3D and 4D offset cases the blade on each rotor produces very similar load spectra with a reduced spectral magnitude in the mid-high frequency range, consistent with the thrust loading results.

As with the single upstream device the azimuthal variation of root bending moment can be calculated and used to determine the influence of the differing onset conditions. The azimuthal variation for the 6D downstream case for the inline and 1D offset case are shown in Figure 17, for one blade on each rotor. These loads have been normalised by the maximum load determined for the single device case, and can be compared directly. In terms of the magnitude of the loads experienced, for all four cases there is a decrease in the loads experienced compared to the single device. For the inline case both rotors experience little variation due to the rotational position, this is as expected as they are positioned directly in the wake, with the vertical shear profile being dominated by the velocity deficit due to the wake. For offset case at 1D, the turbine which is still located in the upstream wake has a similar magnitude to the 0D rotors, but slightly more azimuthal variation with it experiencing some velocity shear. However rotor two has an increase load magnitude due to it's position out of the direct influence of the upstream wake, but the azimuthal variation differs with greater variation at the top of the device, where the wake is still affecting the onset velocity and turbulence characteristics.

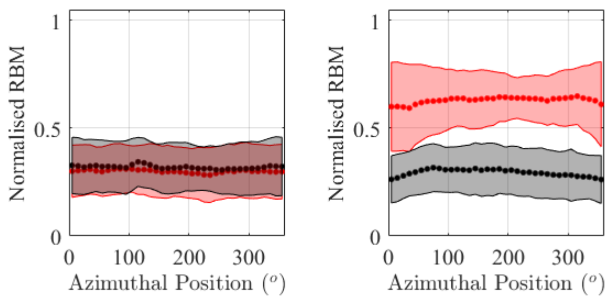

(a) In-line Rotors (b) Offset Rotors

Figure 17: Azimuthal variation of normalised root bending moment for one blade on each rotor in the device for (a) in-line (y =0D) and (b) offset (y=1D) where rotor one (red) and rotor two (black/grey), with solid dots showing mean variation and shaded band for variation within one standard deviation.

5 DISCUSSION

Calculating the variation in loading on a tidal device using an efficient BEM method allows for multiple positions to be considered for the planning of arrays. In order to maximise the potential in a tidal site tidal devices need to be placed within these arrays, where both performance and fatigue need to be considered. Load spectra can be used to determine the aggregated fatigue loads experienced on a component within a device. One of the ways this can be quantified is through a damage equivalent loads (DEL). This load value is calculated based upon the load cycles experienced when the device is operating and a specific material characteristic, which will provide the repeating load the turbine will experience for a given time period. The calculated load cycles can also be used to determine the characteristic cumulative damage, where the number of cycles to failure for a specific material also needs to be known. In this work the the DELs for the inline case and the first offset position are shown in Figure 18.

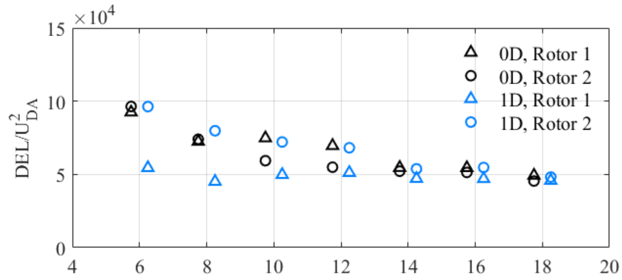

Figure 18: Damage equivalent loads calculated from the thrust loading normalised by the disk averaged velocity, for different downstream positions for the inline case and the offset case at y = 1D, markers are placed either side of each downstream position for clarity, with devices still placed at 6, 8, 10D etc.

Within Figure 18 the calculated damage equivalent load is normalised by the disk averaged velocity at each rotor position. These resultant normalised loads show a variation in magnitude with position. For the inline case, which has experienced the the greatest turbulence intensity and lowest averaged onset flow velocity, the normalised loads are greater in the immediate wake (6-8D). As the device is placed further downstream the normalised loads reduce by 48% to the 18D position. For the inline case the loads experienced on rotor two reduce at a faster rate than rotor one. For the offset case (y = 1D) there is a greater variation in the normalised loads at the positions closest to the upstream device. This is due to the large difference in onset conditions due to one rotor being at the edge of the wake and one rotor being within the wake of the upstream device. As the device moves further downstream this difference in loads reduces to 5% which is comparable to the 6% variation in the inline case, with average difference in loads between these two positions being less than 1%. Considering these loads can be used to determine the design life, with consistent material characteristics, there is little variation in the life span of a component placed at 18 diameters downstream.

6 CONCLUSIONS

For a single tidal device, using the inflow from the LES gives mean rotor loads within 2% and blade loads within 10% between the ALM and BEM methods. There are some minor variations in phase shown in the time-history, however the overall spectra is reproduced well. When examining the azimuthal variation of root bending moment for the BEM method there is around a 2% variation in loading between each rotor.

When considering an additional tidal device placed downstream the variation in onset flow conditions can be determined using an LES simulation, including an upstream device modelled by ALM. The disk averaged velocity and turbulence intensity varies with stream-wise and transverse position, with devices placed in the outer edges of the wake providing conditions closely representing the initial upstream device.

When placing a device inline with the upstream device, considering a stream-wise spacing of 6 rotor diameters there is a reduction in loading due to the velocity deficit from the wake, this can be as great as 35%. Placing a device at an offset position in the wake, can cause each rotor to experience a difference in operating conditions, when the same operating point is chosen, these turbines will also experience a variation in loading, which can be detrimental to design life. This study shows that, even for the relatively complex onset flows that occur within turbine arrays, BEM is a feasible approach to evaluate fatigue loading of tidal turbines at alternative downstream locations in tidal turbine arrays.

ACKNOWLEDGEMENTS

The authors acknowledge the collaboration with Orbital Marine Power Ltd during this work. This research has been financially supported by the EU Interreg project TIGER. Simulations were run using the Computational Shared Facility (CSF) at The University of Manchester (UK).

REFERENCES

Ahmed, U., D. Apsley, I. Afghan, T. Stallard, & P. Stansby (2017). Fluctuating Loads on a Tidal Turbine Due to Velocity Shear and Turbulence: Comparison of CFD with Field Data. *Renewable Energy*, 235–246.

Apsley, D. D. & P. K. Stansby (2020). Unsteady thrust on an oscillating wind turbine: Comparison of blade-element momentum theory with actuator-line CFD. *Journal of Fluids and Structures 98*, 103141.

Díaz-Dorado, E., C. Carrillo, J. Cidras, D. Román, & J. Grande (2021). Performance evaluation and modelling of the Atir marine current turbine. *IET Renewable Power Generation 15*, 821–838.

Garcia-Novo, P. & Y. Kyozuka (2019). Analysis of turbulence and extreme current velocity values in a tidal channel. *Journal of Marine Science and Technology 24*, 659–672.

Harrold, M. & P. Ouro (2019). Rotor Loading Characteristics of a Full-Scale Tidal Turbine. *Energies 12*(6), 1035.

Harrold, M., P. Ouro, & T. O'Doherty (2020). Performance assessment of a tidal turbine using two flow references. *Renewable Energy 153*, 624–633.

Lewis, M., S. Neill, P. Robins, M. Hashemi, & S. Ward (2017). Characteristics of the velocity profile at tidal-stream energy sites. *Renewable Energy 114*, 258–272.

McNaughton, J., S. Harper, R. Sinclair, & B. Sellar (2015). Measuring and Modelling the Power Curve of a Commercial-Scale Tidal Turbine. In *Proceedings of 11th European Wave and Tidal Energy Conference, Nantes, France*, Volume 1, pp. 1–9.

Mercier, P., M. Grondeau, S. Guillou, J. Thiébot, & E. Poizot (2020). Numerical study of the turbulent eddies generated by the seabed roughness. Case study at a tidal power site. *Applied Ocean Research 97*(March), 102082.

Milne, I. A., A. H. Day, R. N. Sharma, & R. G. J. Flay (2016). The characterisation of the hydrodynamic loads on tidal turbines due to turbulence. *Renewable and Sustainable Energy Reviews 56*, 851–864.

Mullings, H. & T. Stallard (2021). Assessment of dependency of unsteady onset flow and resultant tidal turbine fatigue loads on measurement position at a tidal site. *Energies 14*(17), 1–13.

Orbital Marine Power (2022). The O2 Device.

Ouro, P. & T. Nishino (2021). Performance and wake characteristics of tidal turbines in an infinitely large array. *Journal of Fluid Mechanics 925*, A30.

Ouro, P., L. Ramirez, & M. Harrold (2019). Analysis of array spacing on tidal stream turbine farm performance using Large-Eddy Simulation. *Journal of Fluids and Structures 91*(December), 102732.

Ouro, P. & T. Stoesser (2019). Impact of Environmental Turbulence on the Performance and Loadings of a Tidal Stream Turbine. *Flow, Turbulence and Combustion 102*, 613–639.

Parkinson, S. G. & W. J. Collier (2016). Model validation of hydrodynamic loads and performance of a full-scale tidal turbine using Tidal Bladed. *International Journal of Marine Energy 16*, 279–297.

Posa, A. & R. Broglia (2021). Characterization of the turbulent wake of an axial-flow hydrokinetic turbine via large-eddy simulation. *Computers and Fluids 216*, 104815.

Shen, W. Z., R. Mikkelsen, J. N. Sørensen, & C. Bak (2005). Tip loss corrections for wind turbine computations. *Wind Energy 8*, 457–475.

Stallard, T., T. Feng, & P. K. Stansby (2015). Experimental study of the mean wake of a tidal stream rotor in a shallow turbulent flow. *Journal of Fluids and Structures 54*, 235–246.

Stansby, P. & P. Ouro (2022). Modelling marine turbine arrays in tidal flows. *Journal of Hydraulic Research 60*, 187–204.

Togneri, M. & I. Masters (2016). Micrositing variability and mean flow scaling for marine turbulence in Ramsey Sound. *Journal of Ocean Engineering and Marine Energy 2*(1), 35–46.